Journal of Mechanical Engineering and Automation 2014, 4(3): 83-91
DOI: 10.5923/j.jmea.20140403.01

Modelling of Particle Behaviour in Shot Peening Process

Yuki Kato[1], Masaki Omiya[2,*], Hiroaki Hoshino[3]

[1]Graduate School of Science and Technology, Keio University, 3-14-1, Hiyoshi, Kohoku-ku, Yokohama, Kanagawa, 223-8522, Japan
[2]Department of Mechanical Engineering, Keio University, 3-14-1, Hiyoshi, Kohoku-ku, Yokohama, Kanagawa, 223-8522, Japan
[3]Solver Technology Division, Altair Engineering Ltd., 43F Sunshine 60, 3-1-1, Higashi-Ikebukuro, Toshima-ku, Tokyo, 170-6043, Japan

Abstract In this paper, the numerical modelling for particle behaviours in shot peening process is developed with taking account of interactions between particles and treated materials and between particles. Also, particle acceleration by compressive air is considered. The force acting on shot particles is calculated from the detail analysis of the compressive air flow. The developed model is implemented in multi-body dynamic simulator and the particle behaviours in shot peening process are analysed. The numerical results showed that the particle velocity of shot particles before collision is distributed due to the interactions between particles flying from the nozzle to the specimen. Also, the impact location on the specimen surface is distributed, which is the same trend with the experimental results. Therefore, the developed model is simulated the particle behaviours during shot peening. T*he particle velocities and the location of impingement obtained by the proposed approach are useful for the initial condition of the following collision analyses.*

Keywords Shot peening, Multi-body dynamics, Particle behavior, Compressive flow, Impact, Numerical simulation

1. Introduction

Shot peening process has been widely used as one of the most common surface treatments for mechanical and structural components. In this process, a large number of hard shot particles are projected by compressive air at high speed and they impinge on the surface of processed materials. At that time, compressive residual stress and strain hardening are induced in the near surface of treated materials and this treatment improves the fatigue strength of mechanical components.

Shot peening process is very complex phenomena, since a large number of particles hit the specimen surface in a short time. Therefore, the surface modification is difficult to estimate. Recently, numerical approach has been taken to predict the surface modification for shot peening processes. Numerical studies about compressive residual stress induced by shot peening process have been conducted by theoretical based analysis [1] and finite element analyses [2-12]. They focused on the collision behaviour between shot particles and treated materials. The study about shot velocities has been carried out by Ogawa et al. [13], and the analyses of modelling particle behaviours by discrete element method have been developed by Bhuvaraghan et al. [14] and Hong et al. [15]. However, they did not consider the forces from compressive air, which strongly affect the particle behaviour before collision. For the application of erosion testing and abrasive air jet machining, the particle collision and particle streams has been simulated by Ciampini et al. [16], Papini et al. [17] and Li et al. [18]. It is noted that the velocity and the size of shot particle in those application is different from the shot peening process.

The purpose of this paper is to model shot particles before collision and implement the model into multi-body dynamics simulator. The particle behaviour before collision are modelled by considering all forces acting on shot particles, those are drug force from compressive air, the interactive forces between particles. Then, the motion of shot particles are implemented and calculated by multi-body dynamic simulator.

The organization of this paper is followings. To investigate particle behaviours during shot peening in detail, shot peening experiments were carried out. Then, the effects of particle diameter, pressure and the number of particles on impingement behaviours were studied. The developed models were implemented in multi-body dynamics frame work and particle behaviours were simulated and compared with the experimental results.

2. Experimental

2.1. Experimental Set-up

Shot peening experiments were carried out to investigate the effect of shot conditions such as particle diameter, air pressure and the number of particles on the particle behaviours.

The specimen is JIS A5052 (ASTM 5052) aluminium alloy plate. The size of the specimen was 100 mm x 100 mm

* Corresponding author:
oomiya@mech.keio.ac.jp (Masaki Omiya)
Published online at http://journal.sapub.org/jmea

in plane, and the thickness of the specimen was 10 mm. Shot particles were JIS SUJ-2 (ASTM 52100) high carbon-chromium bearing steel and the sphericity of shot particles is 0.5. The experimental apparatus is shown in Figure 1 [19]. Pressure gauge was set at the upper side of compressor tank. The acceleration length in the nozzle, l_n, is 40 mm, and its diameter, d, is 6 mm as shown in Figure 2. Distance from the nozzle tip to the specimen, l, is 100 mm. Shot particles are supplied from the supply inlet of the nozzle. The limitation of the experimental set-up is treated time because the particles are supplied from the inlet by hand. Usually, commercially available shot peening machine shot the particle continually for a long time. However, for this model apparatus, the number of particles in one shot is limited.

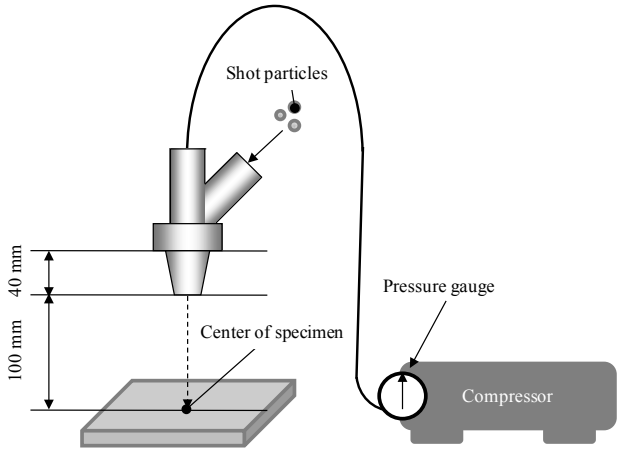

Figure 1. Experimental setup for shot peening process

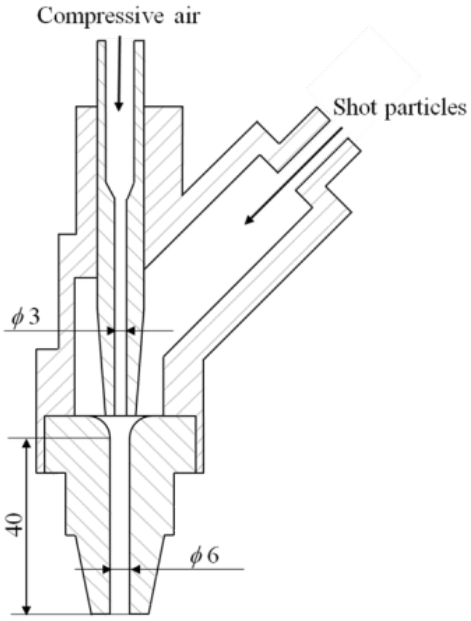

Figure 2. Sectional view of the nozzle

Table 1 shows the experimental conditions. Particle diameter, air pressure and the number of particles at one experiment were changed. From preliminary experiments, the numbers of shot particles were determined. From the indentation of particle impingement on the specimen surface, the spread of shot particles were measured as the distance from the centre of the specimen. The centre of the specimen is set just below the nozzle exit.

Table 1. Experimental conditions

Test No.	Particle diameter, D [mm]	Pressure, P [MPa]	Number of Particles, N
1	0.8	0.6	30
2	0.8	0.6	40
3	0.8	0.3	30
4	0.5	0.6	30
5	0.8	0.6	1

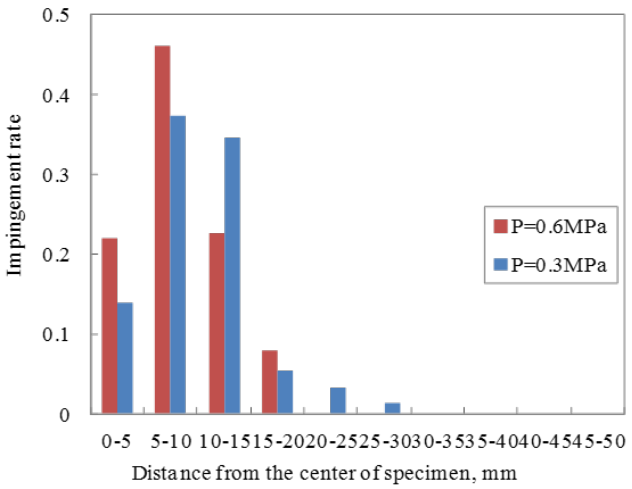

Figure 3. The effect of air pressure on the impact location on specimen

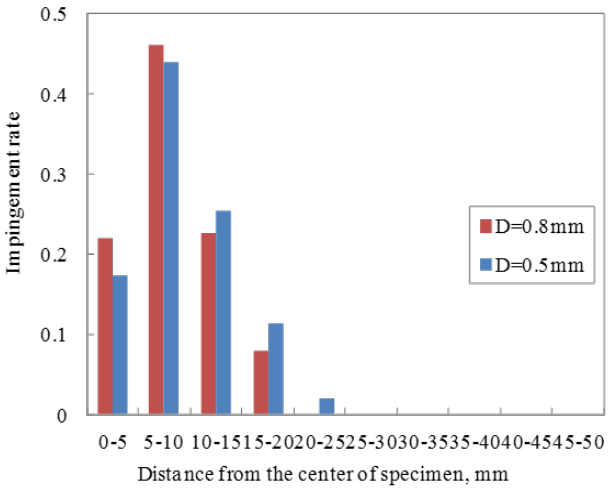

Figure 4. The effect of shot diameter on the impact location on specimen

2.2. Experimental Results

The distance from the indentation of the particle impingement to the centre of specimen was measured by image analyses. The experimental results were shown by histogram of 5 mm intervals from Figure 3 to Figure 5. Figure 3 shows the effect of air pressure on the impact

location. Most particles hit the specimen surface within 20 mm from the centre of specimen. When the air pressure is lower, the surface impact location is broader. Figure 4 shows the effect of shot diameter on the impact location. When the diameter of the shot particle is smaller, the indentation of the particle impingement is broader. Figure 5 also shows the experimental results that single particle experiments and multi-particles experiments are compared. For multi-particles, the impact location is broader due to the collision between particles.

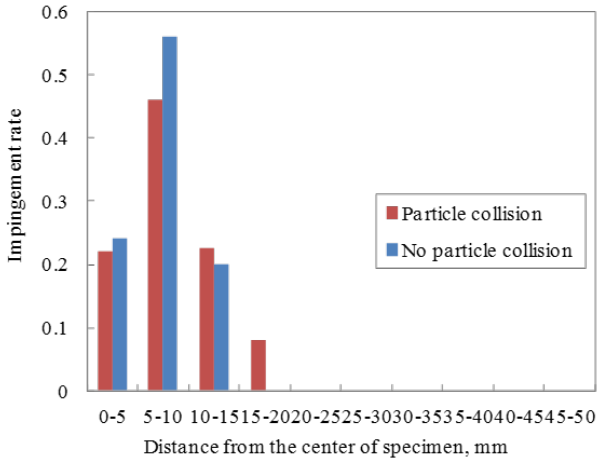

Figure 5. The effect of particle collision on the impact location on specimen

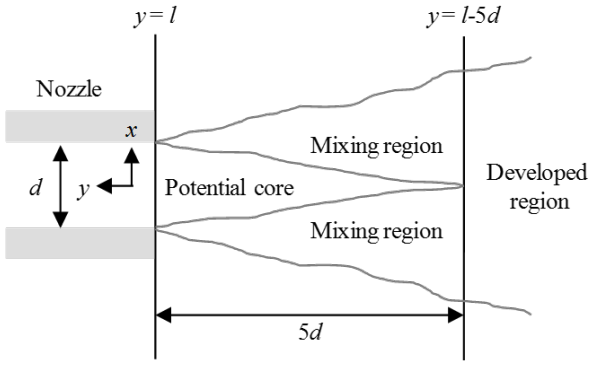

Figure 6. The structure of turbulent jet flow

3. Modeling of Particle Behavior

To make detail modelling about particle behaviours, the jet flow from the nozzle is considered. After blasting air from the nozzle, turbulent jets form three types of regions that are potential core region, mixing region and developed region [18, 20-22]. Particles are accelerated by the jet flow when they pass through these regions. We also focus on the interactive force between particle and specimen and between particles. The interactive force was modelled by using Hertzian contact theory [23, 24].

3.1. Equation of Motion for Shot Particles

The structure of the turbulent jet flows is described in Figure 6 [20, 21]. In its initial stage of development, a region near the nozzle exit and along the center of the jet is called as the potential core region. In this region, mean velocity was assumed to be constant. The region that the potential core region is surrounded with is the mixing region. Over some distance from the nozzle, the jet becomes a fully developed and forms the developed region. The distance at the end of potential core region from the nozzle exit can be described as $5d$, where d is the diameter of the nozzle [21].

When shot particles are passing through these regions, they are accelerated by the drag force from the jet and the equation of motion of particles may be described as [13, 25*]*,

$$m\frac{d^2y}{dt^2} = -\frac{\pi D^2}{8} C_D \rho_a(y)\{u(x,y) - v(x,y)\}^2, \quad (1)$$

where m is the particle mass and C_D is the coefficient of drag. For the spherical shape in turbulent flow, C_D is 0.47 [13, 25]. $\rho_a(y)$ is the air density. D is the particle diameter. u(x, y) is the air velocity and v(x, y) is the particle velocity. The term related to velocities means the relative velocity between air and shot particle. Air density, $\rho_a(y)$, and air velocity, u(x, y), depend on the region where each shot particle is.

Air density in atmosphere, ρ_{ab}, is assumed to be 1.205 Kg/m^3 [25], and air density in the compressor, ρ_{at}, is

$$\rho_{at} = \rho_{ab}\frac{P + P_b}{P_b} = 1.205\frac{P + P_b}{P_b}, \quad (2)$$

where P is the pressure of the compressor and P_b is atmospheric pressure [13]. The air density in the nozzle, ρ_{as}, is obtained as,

$$\rho_{as} = 0.634\rho_{at} = 0.764\frac{P + P_b}{P_b}, \quad (3)$$

Air density in potential core region, $\rho_{ap}(y)$, is equal to air density at compressor, ρ_{at}, as,

$$\rho_{ap}(y) = \rho_{at} = 1.205\frac{P + P_b}{P_b}. \quad (4)$$

Air density in mixing region, $\rho_{am}(y)$, can be derived from the conservation of mass. This relation can be described as,

$$\begin{aligned}\rho_{am}(y) &= -\frac{3}{4}\rho_{as}\left\{1 - \left(\frac{5d}{l-y}\right)^2\right\} \\ &= -0.573\left(\frac{P + P_b}{P_b}\right)\left\{1 - \left(\frac{5d}{l-y}\right)^2\right\}.\end{aligned} \quad (5)$$

Air density in development region, $\rho_{ad}(y)$, can be described as,

$$\rho_{ad}(y) = \rho_{as} - (\rho_{as} - \rho_{ab})\left(\frac{5d}{l-y}\right). \quad (6)$$

By substituting Eq. (3) into Eq. (6),

$$\rho_{\mathrm{a\,d}}(y)=0.764\left(\frac{P+P_{\mathrm{b}}}{P_{\mathrm{b}}}\right)\left(\frac{l-y-5d}{l-y}\right)+1.205\left(\frac{5d}{l-y}\right). \quad (7)$$

3.1.1. Air Velocity in Each Region

If a_0 is the speed of sound and the flow is isentropic, air velocity at the nozzle exit, u_{i}, can be written as,

$$\frac{{u_{\mathrm{i}}}^2}{2}=\frac{{a_0}^2}{\kappa-1}\left\{1-\left(\frac{P_{\mathrm{e}}}{P}\right)^{\frac{\kappa-1}{\kappa}}\right\}, \quad (8)$$

where κ is specific-heat ratio of the compressive air, P is the pressure of compressor and P_{e} is the pressure at the nozzle exit [25]. If the flow is assumed to be a perfect gas and the normal temperature is 293 K, air velocity at the nozzle exit u_{i} is 313.47 m/s.

In the potential core region, air velocity, $u(x,y)$, can be preserved. Thus, air velocity in the potential core region, $u_{\mathrm{p}}(x, y)$, is,

$$u_{\mathrm{p}}(x,y)=u_{\mathrm{i}}. \quad (9)$$

In the mixing region, linear approximation can be applied and the air velocity in the mixing region, $u_{\mathrm{m}}(x, y)$, can be written as,

$$u_{\mathrm{m}}(x,y)=\frac{5u_{\mathrm{i}}}{l-y}\left(x+\frac{y-l-5d}{10}\right). \quad (10)$$

The air velocity in the developed region, $u_{\mathrm{d}}(x, y)$, can also be written as,

$$u_{\mathrm{d}}(x,y)=\frac{6du_{\mathrm{i}}}{l-y}\exp\left\{-94\left(\frac{x}{l-y}\right)^2\right\}. \quad (11)$$

3.1.2. Governing Equations in Each Region

The governing equation of particle motion in the potential core region can be obtained by substituting Eqs. (4) and (9) into Eq. (1) like,

$$m\frac{d^2y}{dt^2}=-\frac{0.47\pi D^2}{8}\left(0.764\frac{P+P_{\mathrm{b}}}{P_{\mathrm{b}}}\right)\left\{u_{\mathrm{i}}-v(x,y)\right\}^2. \quad (12)$$

The governing equation of particle motion in the mixing region can also be obtained by substituting Eqs. (5) and (10) into Eq. (1) like,

$$m\frac{d^2y}{dt^2}=-\frac{0.47\pi D^2}{8}\left(-0.573\left(\frac{P+P_{\mathrm{b}}}{P_{\mathrm{b}}}\right)\left\{1-\left(\frac{5d}{l-y}\right)^2\right\}\right)\left\{\left(\frac{5u_{\mathrm{i}}}{l-y}\right)\left\{x+\frac{y-l-5d}{10}\right\}-v(x,y)\right\}^2. \quad (13)$$

The governing equation of particle motion in the developed region is also obtained by substituting Eqs. (7) and (11) into Eq. (1) like,

$$m\frac{d^2y}{dt^2}=-\frac{0.47\pi D^2}{8}\left\{\begin{array}{l}0.764\left(\frac{P+P_{\mathrm{b}}}{P_{\mathrm{b}}}\right)\left(\frac{l-y-5d}{l-y}\right)\\+1.205\left(\frac{5d}{l-y}\right)\end{array}\right\}\left\{\left(\frac{6du_{\mathrm{i}}}{l-y}\right)\exp\left\{-94\left(\frac{x}{l-y}\right)^2\right\}-v(x,y)\right\}^2. \quad (14)$$

3.2. Horizontal Force Acting on Shot Particles

Horizontal force acting on shot particles was considered after shot particles pass through the nozzle. Streamline of the jet is tilted toward horizontal direction. Angle α in Figure 7, which is the angle between path line and vertical line, means divergence angle. The magnitude of tan α can be obtained from the ratio of air velocity of horizontal direction u_{x} divided by air velocity of vertical direction u_{y}, and this is equal to 0.10.

Weight functions are also set in the jet flow. At the center of the jet, the horizontal force is equal to 0, while the horizontal force at the edge of the jet is equal to 1. Figure 7 shows the weight function. The weight function in the potential core region and mixing region, $f_{\mathrm{t}}(x,y)$, can be described as,

$$f_{\mathrm{t}}(x,y)=\frac{10x}{l-y+5d}. \quad (15)$$

The weight function in the developed region, $f_{\mathrm{d}}(x,y)$, can also be described as,

$$f_{\mathrm{d}}(x,y)=\frac{5x}{l-y}. \quad (16)$$

From these relations, horizontal force in the potential core region and mixing region can be written as,

$$\begin{aligned}m\frac{d^2x}{dt^2}&=m\frac{C_{\mathrm{L}}}{C_{\mathrm{D}}}\frac{d^2y}{dt^2}f_{\mathrm{t}}(x,y)\tan^2\alpha\\&=m\frac{C_{\mathrm{L}}}{C_{\mathrm{D}}}\frac{d^2y}{dt^2}\frac{10x}{l-y+5d}\tan^2\alpha,\end{aligned} \quad (17)$$

where C_{L} is the coefficient of lift. For the spherical shape in turbulent flow, the magnitude of lift coefficient C_{L} varies from 0.03 to 0.3 irregularly [26, 27]. Therefore, lift coefficient C_{L} is assumed to be 0.15.

Horizontal force in the developed region can also be written as,

$$\begin{aligned}m\frac{d^2x}{dt^2}&=m\frac{C_{\mathrm{L}}}{C_{\mathrm{D}}}\frac{d^2y}{dt^2}f_{\mathrm{d}}(x,y)\tan^2\alpha\\&=m\frac{C_{\mathrm{L}}}{C_{\mathrm{D}}}\frac{d^2y}{dt^2}\frac{5x}{l-y}\tan^2\alpha.\end{aligned} \quad (18)$$

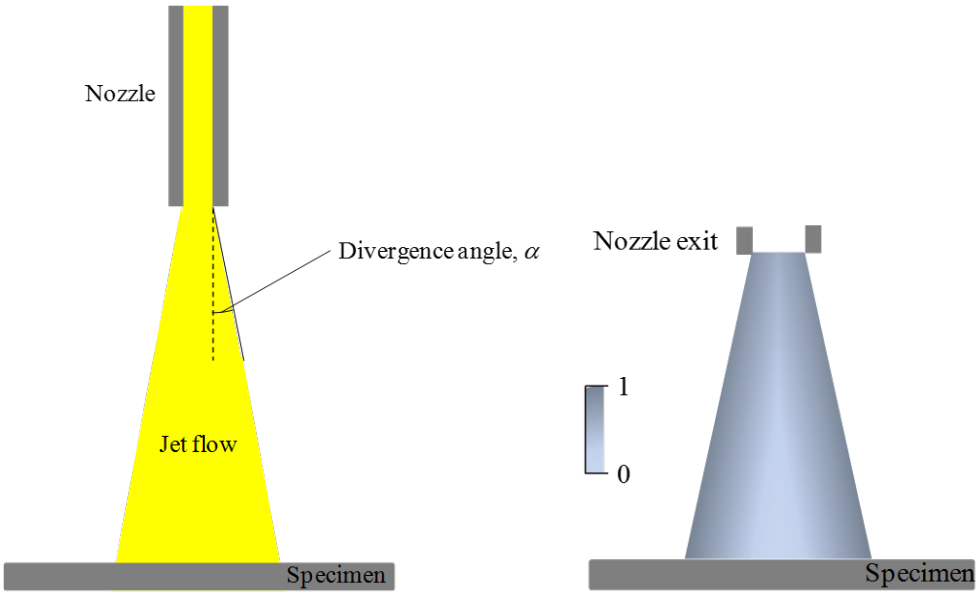

(a) Overall view (b) Contour figure of bias

Figure 7. The divergence of the jet

3.3. Interactive Force between Shot Particle and Specimen

As mentioned above, interactive force between shot particle and specimen can be modelled by Hertzian contact theory [23, 24]. In Hertzian contact theory, contact force can be modelled by non-linear dashpot and non-linear spring as shown in Figure 8. The equation of motion for particles during collision can be described as,

$$m\frac{d^2X}{dt^2} = -K_{PS}X^{\frac{3}{2}} - \eta_{PS}\frac{dX}{dt}, \tag{19}$$

where X is the penetration depth from the contact point, K_{PS} is the coefficient of non-linear spring, and η_{PS} is the damping coefficient.

Non-linear spring coefficient K_{PS} can be written as,

$$K_{PS} = \frac{\frac{4\sqrt{R_P}}{3}}{\frac{1-\nu_P{}^2}{E_P} + \frac{1-\nu_S{}^2}{E_S}}, \tag{20}$$

where R_P is particle radius, ν_P is the Poisson's ratio of particle, E_P is its elastic modulus. ν_S is the Poisson's ratio of specimen, and E_S is its elastic modulus . The damping coefficient η_{PS} can be taken as a fraction of the critical damping $\eta_{critical}$, thus it can be written as,

$$\eta_{PS} = \gamma_{PS}\eta_{critical} = 2\gamma_{PS}\sqrt{mK_{PS}}, \tag{21}$$

by Tsuji et al. [28]. Fraction coefficient γ_{PS} is the function of the coefficient of restitution between shot particle and specimen. The coefficient of restitution between shot particle and specimen e_{PS} can be measured from the freefall test and it was 0.70 in our experimental result, which is similar with the result of Wong et al. [29].

3.4. Interactive Force between Shot Particles

Interactive force between shot particles can also be modelled by Hertzian contact theory [23, 24]. Colliding force between shot particles can also be modeled by dashpot and spring. The equation of motion for particles during collision can be described as,

$$m\frac{d^2X}{dt^2} = -K_{PP}X^{\frac{3}{2}} - \eta_{PP}\frac{dX}{dt}, \tag{22}$$

where X is the penetration depth from the contact point, K_{PP} is the coefficient of non-linear spring, and η_{PP} is the damping coefficient.

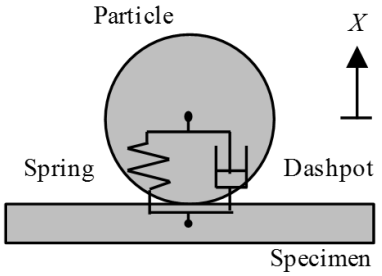

Figure 8. Modelling of Hertzian contact between particle and specimen

Non-linear spring coefficient K_{PP} can be written as,

$$K_{PP} = \frac{\frac{\sqrt{2R_P}}{3}}{\frac{1-\nu_P{}^2}{E_P}}, \tag{23}$$

where R_P is the particle radius, ν_P is the Poisson's ratio of shot particle and E_P is its elastic modulus. The coefficient of non-linear dashpot, η_{PP}, can also be written as,

$$\eta_{PP} = \gamma_{PP}\eta_{critical} = 2\gamma_{PP}\sqrt{mK_{PP}}. \quad (24)$$

Fraction coefficient γ_{PP} is also the function of the coefficient of restitution between shot particles. The coefficient of restitution between shot particles was referred as 0.90 [29, 30].

3.5. Numerical Model and Conditions

The above forces acting on particles were implemented in Multi-body dynamics simulator, MotionSolve (Altiar Engineering) and the equation of motion was solved. Figure 9 shows the numerical model of particle projection. 30 particles set in the side of nozzle randomly. Because there assumed to be the effect of jet entrainment [31], particles were set in the x-direction from 1.5 to 3.0 randomly. The initial velocity of each particle is zero at the nozzle inlet. Governing equation of motion for particles in the nozzle is equal to Eq. (12). Parameters used in numerical simulation are shown in Table 2. Calculations were conducted more than 5 times by changing the initial location of particles.

After projecting compressive air from the nozzle, turbulent jets form the three types of regions as shown in Figure 9 (b). Potential core region comes into effect in the x, y region that meets following conditions.

$$-\frac{y-l+5d}{10} \le x \le \frac{y-l+5d}{10}, l-5d \le y \le l \quad (25)$$

$$-\frac{d}{2} \le x \le \frac{d}{2}, l \le y \le l+l_n \quad (26)$$

Mixing region comes into effect in the x, y region that meets following conditions.

$$\frac{y-l-5d}{10} \le x \le \frac{-y+l-5d}{10}, l-5d \le y \le l \quad (27)$$

$$\frac{y-l+5d}{10} \le x \le \frac{-y+l+5d}{10}, l-5d \le y \le l \quad (28)$$

Developed region also comes into effect in the x, y region that meets following conditions.

$$\frac{y-l}{5} \le x \le \frac{-y+l}{5}, 0 \le y \le l-5d \quad (29)$$

Table 2. Parameters used in numerical simulations

Analysis time, ms	10
Analysis time interval, ms	0.01
Pressure P ,MPa	0.60
Atmospheric pressure P_b ,MPa	0.10
Particle diameter D ,mm	0.8
Particle radius R_s, mm	0.4
Projection length l, mm	100
Nozzle diameter d, mm	6
Nozzle length l_n, mm	40
Poisson's ratio of shot particle ν_s	0.3
Elastic modulus of shot particles E_s, GPa	210
Poisson's ratio of specimen ν_w	0.3
Elastic modulus of specimen E_w, GPa	210
Number of shot particles	30

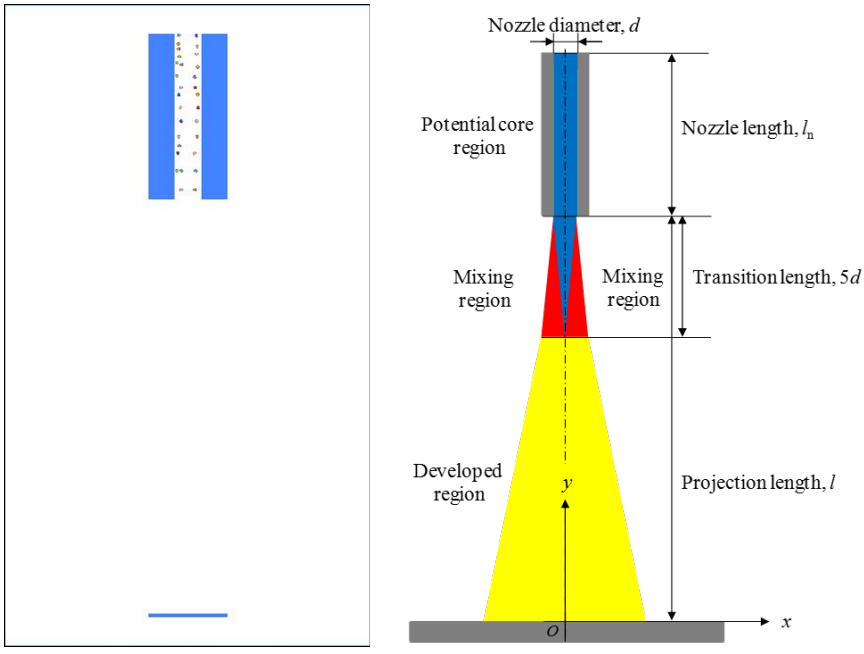

(a) (b)

Figure 9. (a) Initial distribution of shot particles in the nozzle. (b) Overview of turbulent jet

4. Results and Discussion

4.1. Particle Projection

Figure 10 shows particle projection. Due to the interaction between particle and compressive air, particles were accelerated by compressive air depending on where particles pass through in the compressive air region. Figure 11 focuses on the velocity variation from the nozzle inlet to the specimen surface. This is the verification of velocity variation in each region. *Similar velocities has been experimentally observed by Maeda et al.* [32]. In this figure, the case of non-collision between particles and the case of collision among particles are also compared. Velocity of collision particles are varied by the collision between particles.

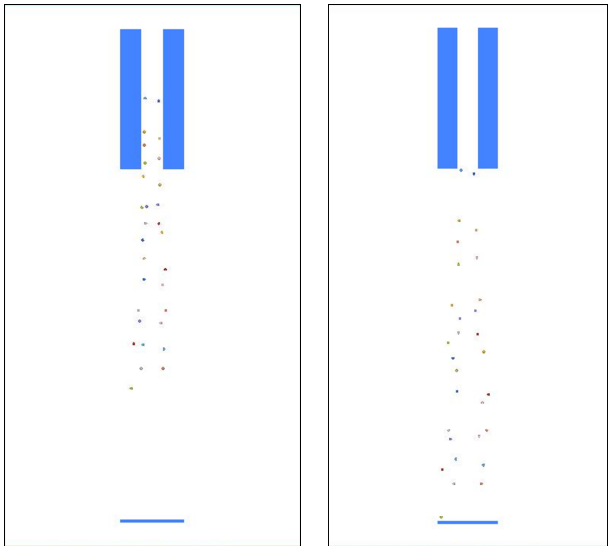

(a) 1 ms (b) 1.5 ms

Figure 10. Particle projection at (a) 1 ms and (b) 1.5 ms

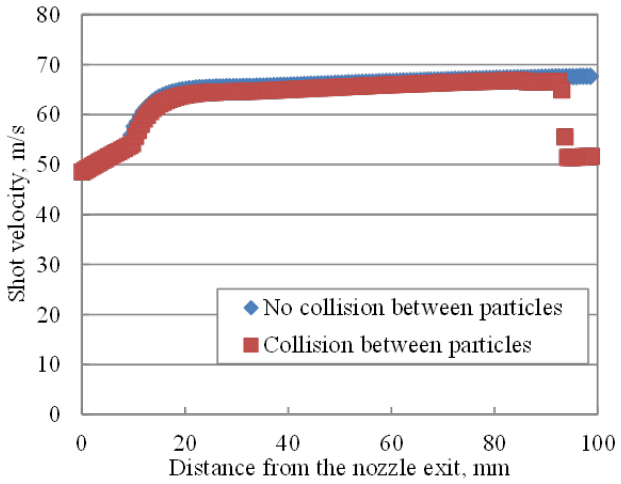

Figure 11. Particle velocity variation

4.2. Particle Velocity and Impingement Location

The particle velocities for y-direction just before impingement are shown by histogram of 5 m/s intervals in Figure 12. About 65% of particles have the velocities between 60 and 80 m/s. But, about 16% of particles were slower than 60 m/s or higher than 80 m/s. Another 19% of particles did not collide with specimen, and their trajectories varied dramatically. This is the effect of the collision among particles. From the calculation of single particle shot, the impingement velocity was about 65 to 70 m/s. When the collisions between particles occur, the particle velocity was changed. Thus, it can be said that the distribution of impingement velocity is due to the collision between particles. Similar trend has been experimentally observed by Shipway and Hutchings [33].

The impact locations of particles were also described by histogram of 5 mm intervals in Figure 13. The peak of the impingement rate is the same as those in Figures 3 to 5. Thus, the numerical model can catch the trend of particle behavior before collision correctly.

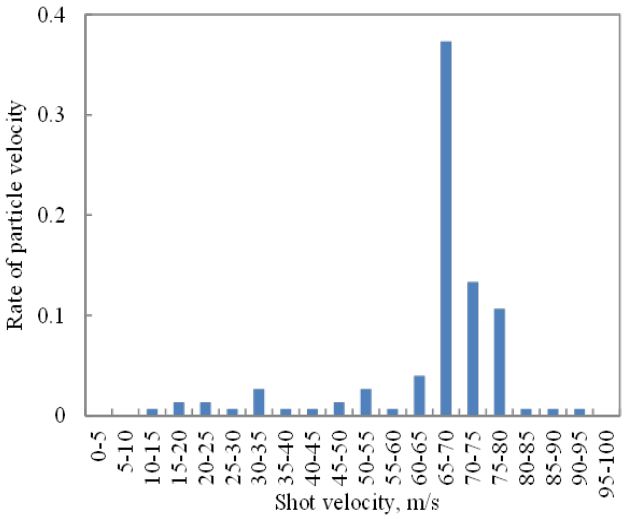

Figure 12. Histogram of impingement velocities of particles

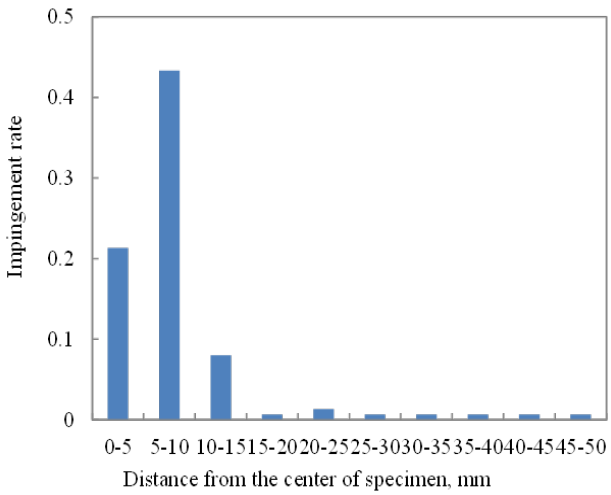

Figure 13. Histogram of impact location of particles

5. Conclusions

In this paper, the numerical simulations of shot peening process by multi-body dynamics were carried out. Special contribution of this paper is the detail modelling about the interaction between shot particles and compressive air. Particle interactions are also modeled by Hertzian contact theory. The numerical results were compared with the experimental results. Results obtained in this paper are summarized as the followings.

1. Considering acting forces on the shot particle from the jet flow of compressive air, equation of motion was derived and implemented in multi-body dynamics simulation.
2. Distribution of impingement velocity can be found. This phenomenon is caused by the collision between particles.
3. Distribution of particle impingement location can also be observed. The peak of the impingement rate is 5 to 10 mm from the center of the nozzle. This result is identical to the experimental results.

The particle velocities and the location of impingement obtained by the proposed approach are useful for the initial condition of the following collision analyses, such as finite element analyses.

The future work of this study is the direct comparison between experimental and numerical results. The shot particles can be observed by a high speed camera and the results will be reported elsewhere [34].

ACKNOWLEDGEMENTS

The authors acknowledge the Academic Open Program of Altair Engineering Inc. for using HyperWorks software.

REFERENCES

[1] K. Ogawa, T. Asano, Theoretical Prediction of Residual Stress Induced by Shot Peening and Experimental Verification for Carburized Steel, *Japan Society of Materials Science*, 48 (1999) 1360-1366.

[2] T. Hong, J.Y. Ooi, B. Shaw, A numerical study of the residual stress pattern from single shot impacting on a metallic component, *Advances in Engineering Software*, 39 (2008) 743-756.

[3] M. Guagliano, Relating Almen intensity to residual stress induced by shot peening: a numerical approach, *Journal of Materials Processing Technology*, 110 (2001) 277-286.

[4] G.I. Mylonas, G. Labeas, Numerical modeling of shot peening process and corresponding products: Residual stress, surface roughness and cold work prediction, *Surface and Coatings Technology*, 205 (2011) 4480-4494.

[5] B. Bhuvaraghan, S.M. Srinivasan, B. Maffeo, Numerical simulation of Almen strip response due to random impacts with strain-rate effects, *International Journal of Mechanical Sciences*, 53 (2011) 417-424.

[6] B. Yildirim, S. Muftu, A. Gouldstone, Modeling of high velocity impact of spherical particles, *Wear*, 270 (2011) 703-713.

[7] A. Gariepy, S. Larose, C. Perron, M. Levesque, Shot peening and peen forming finite element modeling – Towards a quantitative method, *International Journal of Solids and Structures*, 48 (2011) 2859-2877.

[8] H.Y. Miao, S. Larose, C. Perron, M. Levesque, On the potential applications of a 3D random finite element model for the simulation of shot peening, *Advances in Engineering Software*, 40 (2009) 1023-1038.

[9] T. Kim, J.H. Lee, H. Lee, S. Cheong, An area-average approach to peening residual stress under multi-impacts using a three-dimensional symmetry-cell finite element model with plastic shots, *Materials and Design*, 31 (2010) 50-59.

[10] H.Y. Miao, S. Larose, C. Perron, M. Levesque, An analytical approach to relate shot peening parameters to Almen intensity, *Surface and Coatings Technology*, 205 (2010) 2055-2066.

[11] G.H. Majzoobi, R. Azizi, A. Alavi Nia, A three-dimensional simulation of shot peening process using multiple shot impacts, *Journal of Material Processing Technology*, 164-165 (2005) 1226-1234.

[12] S.M. Hassani-Gangaraj, M. Guagliano, G.H. Farrahi, Finite element simulation of shot peening coverage with the special attention on surface nanocrystallization, *Procedia Engineering*, 10 (2011) 2464-2471.

[13] K. Ogawa; T. Asano; A. Saito; K. Kawamura; M. Ogino; H. Aihara: Measurement and Analysis of Shot Velocity in Pheumatic Shot Peening. *Transactions of the Japan Society of Mechanical Engineers*, 60 C (1994) 1120-1125.

[14] B. Bhuvaraghan, S.M. Srinivasan, B. Maffeo, R.D. McCLain, Y. Potdar, O. Prakash, Shot peening simulation using discrete and finite element methods, *Advances in Engineering Software*, 41 (2010) 1266-1276.

[15] T. Hong, J.Y. Ooi, B. Shaw, A numerical simulation to relate the shot peening parameters to the induced residual stresses, *Engineering Failure Analysis*, 15 (2008) 1097-1110.

[16] D. Ciampini, J.K. Spelt, M.Papini, Simulation of interference effects in particle streams following impact with a flat surface Part I. Theory and analysis, *Wear*, 254 (2003) 237-249.

[17] M. Papini, D. Ciampini, T. Krajac, J.K. Spelt, Computer modelling of interference effects in erosion testing: effect of plume shape, *Wear,* 255 (2003) 85-97.

[18] H.Z. Li, J. Wang, J.M. Fan, Analysis and modelling of particle velocities in micro-abrasive air jet, *International Journal of Machine Tools & Manufacture,* 49 (2009) 850-858.

[19] ISO 26910-1:2009, Springs – Shot peening – Part 1: General procedures.

[20] N. Rajaratnaum, Turbulent Jets, Elsevier, 1976.

[21] T. Shakouchi, Jet Flow Engineering –Fundamentals and Application–, Morikita, 2004.

[22] A. Sarkar, R.P. Singh, Air impingement technology for food

processing: visualization studies, Lebensmittel-*Wissenschaft und-Technologie*, 37 (2004) 873-879.

[23] K.L. Johnson, Contact Mechanics, Cambridge University Press, 1985.

[24] D. Maugis, Contact Adhesion and Rupture of Elastic Solids, Springer, 203 (1999).

[25] F.M. White, Fluid Mechanics, Six Edition, McGraw-Hill, 2008.

[26] K. Aoki, K. Muto, H. Okanaga, Effects of dimples for drag and lift on a sphere with rotation, *Transactions of the Japan Society of Mechanical Engineers*, 77 C (2011) 793-802.

[27] J.B. Barlow, M.J. Domanski, Lift on stationary and rotation spheres under varying flow and surface conditions, *AIAA Journal*, 46 (2008) 1932-1936.

[28] Y. Tsuji, T. Tanaka, T. Ishida, Lagrangian numerical simulation of plug flow of cohesionless particles in a horizontal pipe, *Powder Technology*, 71 (1992) 239-250.

[29] C.X. Wong, M.C. Daniel, J.A. Rongong, Energy dissipation prediction of particle dampers, *Journal of Sound and Vibration*, 319 (2009) 91-118.

[30] A. Aryaei, K. Hashemnia, K. Jafarpur, Experimental and numerical study of ball size effect on restitution coefficient in low velocity impacts, *International Journal of Impact Engineering*, 37 (2010) 1037-1044.

[31] D.J. Tritton, Physical Fluid Dynamics, Second Edition, Oxford University Press, 1988.

[32] H. Maeda, N. Egami, C. Kagaya, N. Inoue, H. Takesita, K. Ito, Analysis of Particle Velocity and Temperature Distribution of Struck Surface in Fine Particle Peening, *Transactions of the Japan Society of Mechanical Engineers*, 67 C (2001) 306-312.

[33] P.H. Shipway, I.M. Hutchings, A method for optimizing the particle flux in erosion testing with a gas-blast apparatus, *Wear*, 174 (1994) 169-175.

[34] Y. Aiba, K. Murai, M. Omiya, J. Komotori, Observation of Particle Behavior in Fine Particle Peening process, *Proceedings of 12th International Conference on Shot Peening (ICSP2014), Goslar, Germany, September 15-18*, (2014).